Climate Dynamics (2019) 52:4351–4369
https://doi.org/10.1007/s00382-018-4383-0

Interannual variability and dynamics of intraseasonal wind rectification in the equatorial Pacific Ocean

Xia Zhao[1,2] · Dongliang Yuan[1,2,5] · Guang Yang[3,4] · Jing Wang[1,2] · Hailong Liu[6] · Renhe Zhang[7] · Weiqing Han[8]

Received: 22 December 2017 / Accepted: 3 August 2018 / Published online: 9 August 2018

Abstract
The rectification of intraseasonal wind forcing on interannual sea surface temperature anomalies (SSTA) and sea level anomalies (SLA) associated with El Niño–Southern Oscillation (ENSO) during 1993–2016 are investigated using the LICOM ocean general circulation model forced with daily winds. The comparisons of the experiments with and without the intraseasonal wind forcing have shown that the rectified interannual SSTA and SLA by the intraseasonal winds are much weaker than the total interannual SSTA and SLA in the cold tongue, due to the much weaker rectified than the total interannual Kelvin and Rossby waves in the equatorial Pacific Ocean. The dynamics of the rectification are through the nonlinear zonal and vertical advection by the background currents, which produces downwelling equatorial Kelvin waves during El Niño. The meridional advection is much smaller than the zonal and vertical advection, suggesting that the rectification is not induced by the Ekman dynamics or the thermocline rectification. The rectified interannual Kelvin waves are found to be much smaller than reflected at the Pacific western boundary and those forced by the interannual winds, suggesting that the latter two play a much more important role in ENSO dynamics than the intraseasonal winds. The results of this study suggest an unlikely significant role of oceanic nonlinear rectification by intraseasonal winds during the onset and cycling of El Niño.

Keywords Intraseasonal rectification · Interannual variability · ENSO · Kelvin and Rossby waves · Nonlinear oceanic dynamics

1 Introduction

The El Niño–Southern Oscillation (ENSO) is the climate mode that dominates interannual variability in the tropical Pacific ocean–atmosphere coupled system, which has global repercussions. The initiation of the ENSO events is still an issue unsettled to date. Early observations suggest that westerly wind bursts (Luther et al. 1983) play the potential role of triggering the El Niño events. The study of Lukas et al. (1984) shows strong westerly wind bursts during the onset of the 1982–1983 El Niño, forcing significant downwelling equatorial Kelvin waves to the eastern equatorial Pacific. The effect of the westerly wind bursts is enhanced by the existence of a shallow mixed layer above an oceanic barrier layer in the western Pacific Ocean (Lukas and Linstrom 1991), which traps the momentum of the surface wind forcing in a thin surface layer. Significant intraseasonal westerly wind bursts have indeed been observed to precede major El Niño events (e.g. Moore and Kleeman 1999; McPhaden 1999; Lengaigne et al. 2004a, b; Menkes et al. 2014; Fedorov et al. 2014; Chen et al. 2015; Hu and Fedorov 2016). These observations have made people to hypothesize that intraseasonal westerly winds play an important role in triggering El Niño.

Observations have shown that the tropical atmosphere variations contain strong intraseasonal variability (10–90 days periods), the most prominent of which is the so-called Madden–Julian Oscillations (MJO; Madden and Julian 1971, 1972). The MJO usually originate and grow in the tropical Indian Ocean and propagate to the western and central equatorial Pacific year round, with clear signatures in troposphere zonal winds and tropical deep convection. Both westerly and easterly wind bursts are generated during the passages of the MJO events. Strong MJO events are observed every year to frequent the tropical western Pacific Ocean (e.g. Kessler et al. 1995; McPhaden 1999; Bergman et al. 2001; Zhang and Gottschalck 2002; Roundy and Kiladis 2006; Hendon et al. 2007). Why some of the MJO events trigger El Niño while some others do not? It is known

✉ Dongliang Yuan
dyuan@qdio.ac.cn

Extended author information available on the last page of the article

that the simultaneous correlation between the interannual MJO and the cold tongue sea surface temperature anomalies (SSTA) is very weak during northern winter (e.g. Slingo et al. 1999; Hendon et al. 1999), suggesting that the two are often not associated with each other. Some coupled model simulations have indeed shown that the atmospheric intraseasonal variability has little influence on ENSO evolution (e.g. Zebiak 1989).

ENSO and the intraseasonal variations are tropical oscillations at very disparate frequencies, the interactions of which must go through nonlinear dynamics in the atmosphere or/and ocean. Kessler and Kleeman (2000) use a harmonic representation of the intraseasonal wind stress over the western equatorial Pacific to force an ocean general circulation model (OGCM). Their simulations suggest that the intraseasonal winds rectify interannual anomalies through oceanic nonlinearity, which produce low-frequency SSTA of about 0.1 °C in the central Pacific. However, SSTA of ~0.1 °C in the central-eastern equatorial Pacific are much smaller than the interannual SSTA associated with El Niño and are unlikely important even during the onset of an El Niño. Due to the idealized configurations of their forcing, realistic SSTA rectified in the cold tongue have not been estimated. Rong et al. (2011) have estimated the rectified SSTA by the observed intraseasonal winds using an OGCM, showing slightly larger, yet still small, SSTA rectified through oceanic nonlinearity in the eastern equatorial Pacific.

The dynamics of the SSTA rectification remain unclear to date. Observations suggest that the intraseasonal wind forcing is concentrated over the western equatorial Pacific, which shall rectify the cold tongue interannual SSTA through the propagation of the interannual long equatorial Kelvin waves. Two kinds of dynamics are potentially involved in the generation of the rectified equatorial Kelvin waves. One is the meridional advection due to the surface Ekman transports of the intraseasonal zonal winds (Kessler and Kleeman 2000); the other is the thermocline depth rectification due to the Ekman pumping (Yuan and Liu 2009). The former generates downwelling Kelvin waves whereas the latter generates upwelling Kelvin waves after one cycle of harmonic wind forcing. In the equatorial Indian Ocean, Yuan and Liu (2009) have shown that the intraseasonal winds rectify upwelling Kelvin waves, which are very weak and are unlikely to play a significant role in the interannual dynamics. The rectified interannual Kelvin waves in the tropical Pacific Ocean have not been evaluated so far.

Several mechanisms have been proposed to produce the ENSO cycling. Among them the delay oscillator (Suarez and Schopf 1988), the discharge–recharge oscillator (Jin 1997a, b), the advective-reflective oscillator (Picaut et al. 1997), and the western Pacific oscillator (Weisberg and Wang 1997), all have suggested that the reflections of the oceanic equatorial Rossby waves at the Pacific western boundary play an important role in terminating ENSO (e.g. Schopf and Suarez 1988; Boulanger and Menkes 1999; Boulanger et al. 2003; Yuan et al. 2004). The roles of the oceanic Kelvin waves generated by the intraseasonal wind forcing and by the Rossby wave reflection at the Pacific western boundary during the onset and terminating phases of ENSO have not been compared to date.

In this study, a series of forced OGCM experiments with and without intraseasonal wind forcing are conducted. The rectified Kelvin waves are evaluated based on these experiments and are compared with the interannual oceanic Kelvin waves forced by the low-frequency winds and reflected at the western boundary, based on which the role of the intraseaonal wind forcing in ENSO dynamics is evaluated. The purpose of this study is different from that of Rong et al. (2011) in that we focus on the rectified equatorial Kelvin waves linking the intraseasonal wind forcing in the western-central equatorial Pacific with the interannual SSTA in the eastern basin. The rectification through the oceanic nonlinearity is found to be small and unlikely to play a significant role in ENSO initiation and termination.

The remainder of this manuscript is organized as the following. The model and data in this study are introduced in Sect. 2. Results of the model simulation are validated in Sect. 3. The rectification by the intraseasonal wind forcing during ENSO is estimated, the role of which is evaluated in Sect. 4. The dynamics of the oceanic nonlinear rectification are investigated in Sect. 5. Discussions and conclusions are summarized in Sect. 6.

2 Modal and data

The OGCM used in this study is the Laboratory of Numerical Modeling for Atmospheric Sciences and Geophysical Fluid Dynamics (LASG)/Institute of Atmospheric Physics (IAP) Climate System Ocean Model (LICOM; Liu et al. 2004, 2005). The LICOM model employs a free sea surface and nearly leveled vertical coordinates in the deep ocean (the η coordinate) and contains complete dynamics of the ocean circulation. The domain of the model covers the global ocean between 78.5°S and 90°N with a horizontal resolution of 0.5° latitude by 0.5° longitude. There are 30 levels in the vertical with 12 layers in the upper 300 m. The Packnowski and Philander (1981) mixing scheme is used to represent the enhanced vertical mixing in the surface layer. A 900-year spin-up simulation is conducted from the initially motionless ocean and climatological temperature and salinity based on the World Ocean Atlas dataset of 1994 (Levitus and Boyer 1994; and Levitus et al. 1994).

Four sets of numerical experiments using different surface wind forcings are conducted to estimate the rectification of the intraseasonal winds on the SSTA and sea level

anomalies (SLA) at the interannual time scales. A main-run control experiment (hereafter MR) is forced with the daily wind stress and heat flux of the National Center for Environmental Prediction–National Center for Atmospheric Research (NCEP–NCAR) reanalysis (Kalnay et al. 1996) during 1948–2016. The surface wind stress, latent and sensible heat fluxes, long wave and short wave radiation are calculated using the formula of Large and Yeager (2004, 2009). The surface wind stress and latent and sensible heat fluxes are based on the daily winds, air temperature, and specific humidity at 10 m above the sea surface and the model sea surface temperature (SST). According to Shinoda et al. (2008), intraseasonal winds of the NCEP–NCAR reanalysis agree well with in situ and scatterometer measurements in the western Pacific. In this study, we focus on the rectification of the intraseasonal wind forcing on the interannual SSTA and SLA associated with ENSO.

An experiment called EXP1 is conducted to force the same ocean model with low-passed wind stress over the tropical oceans of the globe (20°N–20°S). The cut-off period of the low-pass filter is 90 days, so that the intraserasonal wind stress is excluded in Experiment EXP1. The latent and sensible heat fluxes are the same in the MR. The effects of intraseasonal wind stress on the SSTA and SLA are evaluated by substracting EXP1 from MR and comparing the differences with the MR simulations.

Due to the nonlinear quadratic relation in the bulk formula of the wind tress calculation, low frequency wind stress can be rectified by high frequency wind variability. To examine this effect, the daily wind velocity components are low-passed with the same Gaussian filter (using the Lanczos filter shows similar results), based on which, the low-frequency wind stress is calculated. Experiment EXP2 is conducted to force the model with this low frequency wind stress over the tropical oceans of the globe (20°N–20°S). The latent and sensible heat fluxes are calculated using the unfiltered winds so that they are the same as in MR and EXP1.

To isolate the rectification of the intraseasonal winds through the heat flux, low-passed daily winds are used to calculate the wind stress, and latent and sensible heat fluxes, which are used to force the model in Experiment EXP3. The difference between EXP2 and EXP3 measures the rectification of intraseasonal winds through the heat fluxes.

The LICOM model simulations have been decomposed into equatorial waves to estimate the effects of the intraseasonal rectification on the evolution of ENSO. The eigenfunctions and wave speeds of the baroclinic modes are calculated based on the averaged density profile over the equatorial Pacific Ocean between 5°S and 5°N. The three-dimensional dynamic height and zonal velocity referenced to 2500 m depth of no motion are projected onto the eigenfunctions to extract the baroclinic modes, which are further decomposed into equatorial Kelvin and Rossby waves using the method described by Yuan et al. (2004). The decomposed Kelvin and Rossby waves preserve the model nonlinearity. Yuan et al. (2004) have found that the reflection of the Kelvin waves at the Pacific eastern boundary is in good agreement with a linear reflection at a straight wall, while the reflection of the Rossby waves at the Pacific western boundary is significantly different from the linear theory.

The SST data used in this study is the Hadley Center data (HadISST; Rayner et al. 2003) compiled on a 1° longitude by 1° latitude grid based on in situ and satellite observations. The merged sea surface height anomalies are the satellite altimeter measurements onboard of Satellites Topex/Poseidon, ERS, and Jason-1 since 1993, which are calibrated, merged, and archived by the AVISO project (ftp://ftp.aviso.oceanobs.com). Because of the SLA data, the analyses of the LICOM hindcast in this study focus on the period from 1993 to 2016.

3 Validation of the MR simulation

The simulated SSTA and SLA are compared with the observations in this section, based on which the MR solution is decomposed into equatorial waves to study the ENSO dynamics.

3.1 Comparison with the observation

The area-averaged SSTA time series in the Nino 3 region (150°W–90°W, 5°S–5°N) of the MR simulation are found to be in good agreement with the Hadley Center data (Fig. 1), suggesting that the low-frequency signals of SST, especially those at the seasonal and interannual time scales, are reproduced well by the simulation. The correlation and root-mean-square error (RMSE) between the simulated and Hadley center data are 0.93 and 0.5 °C, respectively. The comparison of the simulated SSTA averaged between 5°S and 5°N over the equatorial Pacific Ocean of the MR with the Hadley Center data shows that the abnormal warmings during the 1994–1995, 1997–1998, 2002–2003, 2006–2007, 2009–2010, and 2015–2016 El Niño events in the central and eastern equatorial Pacific have been reproduced well by the OGCM (Fig. 2). The abnormal coolings of the central and eastern equatorial Pacific during the 1995–1996, 1998–2001, 2007–2008, 2010–2011 La Niña events also compare well with the Hadley Center data. These comparisons suggest that the model can be used as a proxy to estimate the effects of the rectification on the SSTA in the cold tongue and the associated dynamics by the intraseasonal forcing.

The simulated sea level anomalies (SLA) of the MR are validated with the AVISO satellite altimeter data (Fig. 3). The positive (negative) SLA in the eastern (western)

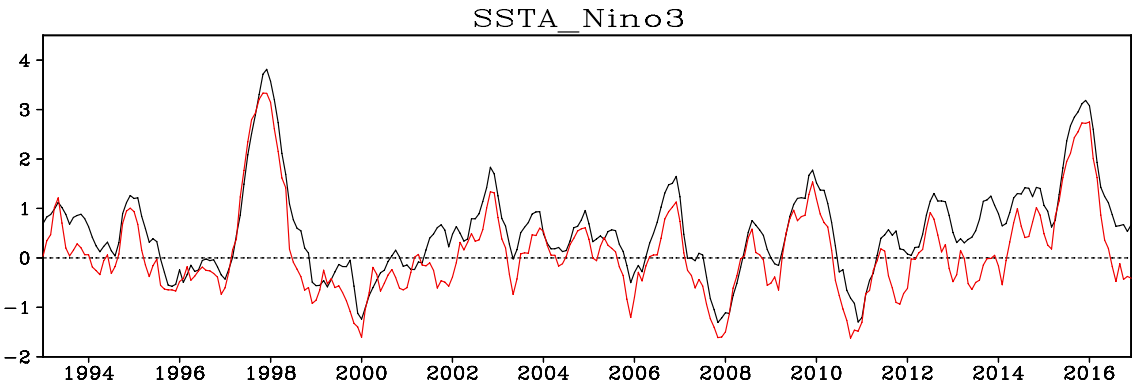

Fig. 1 Comparison of simulated monthly SSTA time series in Nino 3 region of the MR (black curve) with the Hadley Center data (red curve)

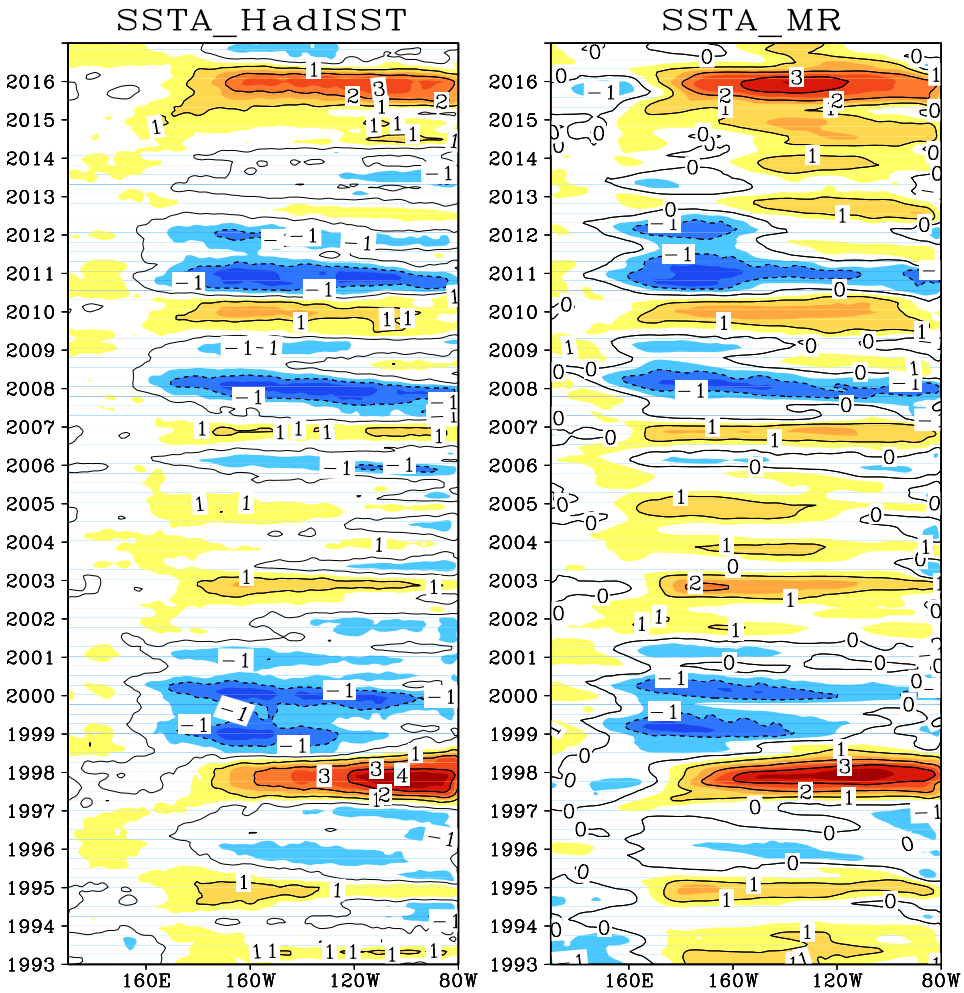

Fig. 2 Comparison of monthly averaged SSTA between 5°S and 5°N over the equatorial Pacific Ocean of the MR (right panel) with the Hadley Center data (left panel). Red (blue) color indicates SSTA greater (less) than 0.5 (−0.5) °C and the contour interval is 1 °C

equatorial Pacific Ocean during the 1994–1995, 1997–1998, 2002–2003, 2006–2007, 2009–2010 and 2015–2016 El Niño events have been reproduced by the OGCM. The simulated SLA during the 1995–1996, 1998–2001, 2007–2008, 2010–2011 La Niña events also compare well with the altimetry data. The simulated SLA during the 1997–1998 and the 2015–2016 strong El Niños are noticeably weaker than the altimeter data, which may be due to errors of the wind stress or/and model dynamics. The correlation and RMSE between the simulated SLA and AVISO data in the

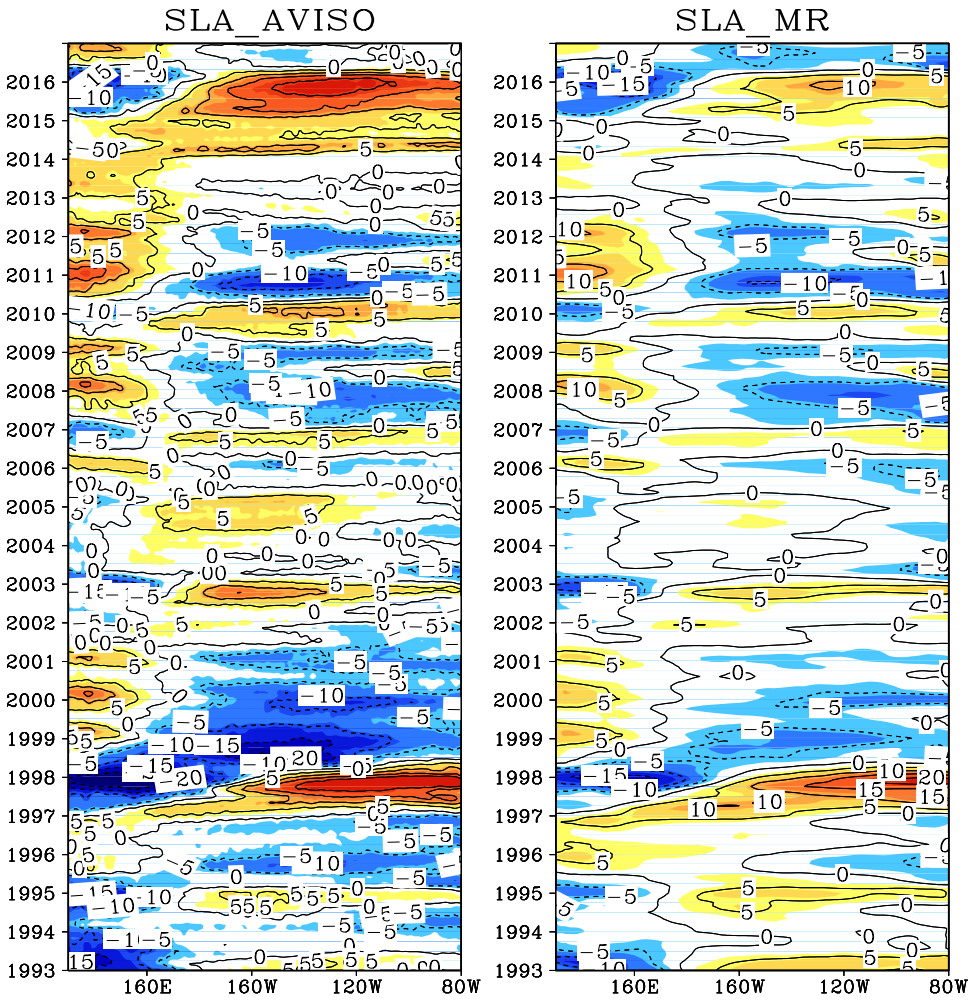

Fig. 3 Comparison of monthly averaged sea level anomalies (SLA) between 5°S and 5°N of the MR (right panel) with the AVISO altimeter data (left panel). Red (blue) color indicates SLA greater (less) than 3 (−3) cm, and the contour interval is 5 cm

Nino 3 region are 0.89 and 3.5 cm, respectively. The comparisons of the simulated SSTA and SLA with observations suggest that the model can be used to study the dynamics of the equatorial Pacific Ocean circulation during the ENSO events of 1993–2016.

3.2 Equatorial waves in MR

To study the interannual equatorial wave dynamics of the ENSO events, the MR solution is decomposed into long equatorial waves. The longitude-time plots of the Kelvin wave coefficients of the first baroclinic mode (Fig. 4) show the eastward propagating downwelling Kelvin waves in 1994, 1997, 2002, 2006, 2009, and 2015, forced by the westerly winds anomalies near the dateline (Fig. 5). The downwelling Kelvin waves in the far western equatorial Pacific in 1997, 2006, and 2009 are evidently reflected from the downwelling Rossby waves at the western boundary (Fig. 4). These eastward propagating downwelling Kelvin waves deepen the thermocline in the eastern equatorial Pacific, which are responsible for the onset of positive SSTA in the central and eastern equatorial Pacific during the 1994–1995, 1997–1998, 2002–2003, 2006–2007, 2009–2010, and 2015–2016 El Niño events. Upwelling Rossby waves are also generated by the same westerly wind anomalies near the dateline, which propagate to the western boundary and get reflected into upwelling Kelvin waves at later times after the downwelling Kelvin wave propagations (Fig. 4). These upwelling Kelvin waves serve to weaken the thermocline depth anomalies in the central and eastern equatorial Pacific, resulting in a decrease of the SSTA and SLA (Figs. 2, 3). Our simulation is consistent with the results of Yuan et al. (2004), showing that the western boundary reflection plays an important role in the decay and termination of the El Niño events since 1993.

Westward propagation of the downwelling Rossby waves during the 1995–1996, 1998–1999, 1999–2000, 2000–2001, 2007–2008, 2010–2011 La Niña events (Fig. 4) is forced by the easterly wind anomalies near the dateline (Fig. 5). These Rossby waves propagate to the western boundary and are reflected into downwelling Kelvin waves (Fig. 4). These downwelling Kelvin waves must be reflected from the

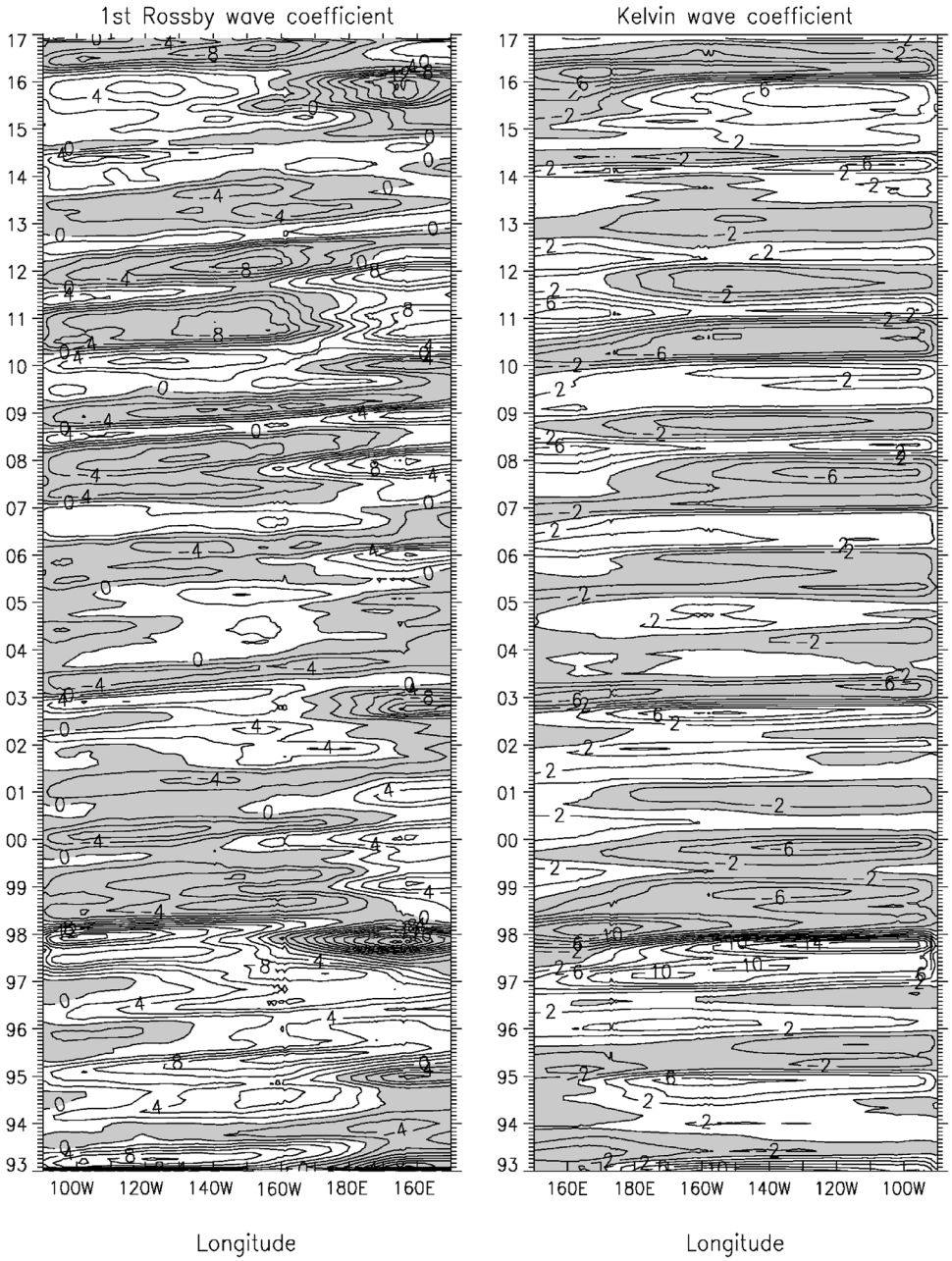

Fig. 4 Decomposed coefficients of equatorial Kelvin and the first meridional mode Rossby waves of the first baroclinic mode for the results of MR. Shading indicates the negative values, and the contour interval is 2

Rossby waves at the western boundary because they cannot be forced by the easterly wind anomalies over the western-central equatorial Pacific at the same time (Fig. 5). The eastward propagation of those downwelling Kelvin waves is visible at the end of 1995, 1998, 1999, 2000, 2007, 2010. Among them, the Kelvin waves propagating to the central and eastern Pacific at the beginning of 1996, 2001, 2008, and 2011 weaken the cooling in the eastern Pacific until it vanishes or reverted into warming. Thus, the Rossby wave reflections at the Pacific western boundary provide a crucial negative feedback for the termination of the La Niña events.

The decomposed Kelvin waves have been compared with the linearly reflected Kelvin waves calculated from the decomposed Rossby waves of the first baroclinic mode at the western boundary in the MR (Fig. 6). The details have been described by Yuan et al. (2004). The dotted curve in Fig. 6 is calculated from the incoming equatorial Rossby waves of meridional modes 1 and 3 (symmetric), and the dashed curve adds the contribution from the meridional modes 2 (anti-symmetric). The ratios of linear reflection at the western boundary are 0.41, 0.6, and 0.13 for the interannual Rossby waves of meridional modes 1, 2, and 3, respectively. Higher meridional-mode Rossby waves make negligible contributions to the Kelvin wave amplitude. The significant difference between the decomposed Kelvin waves and reflected Kelvin waves based on the linear

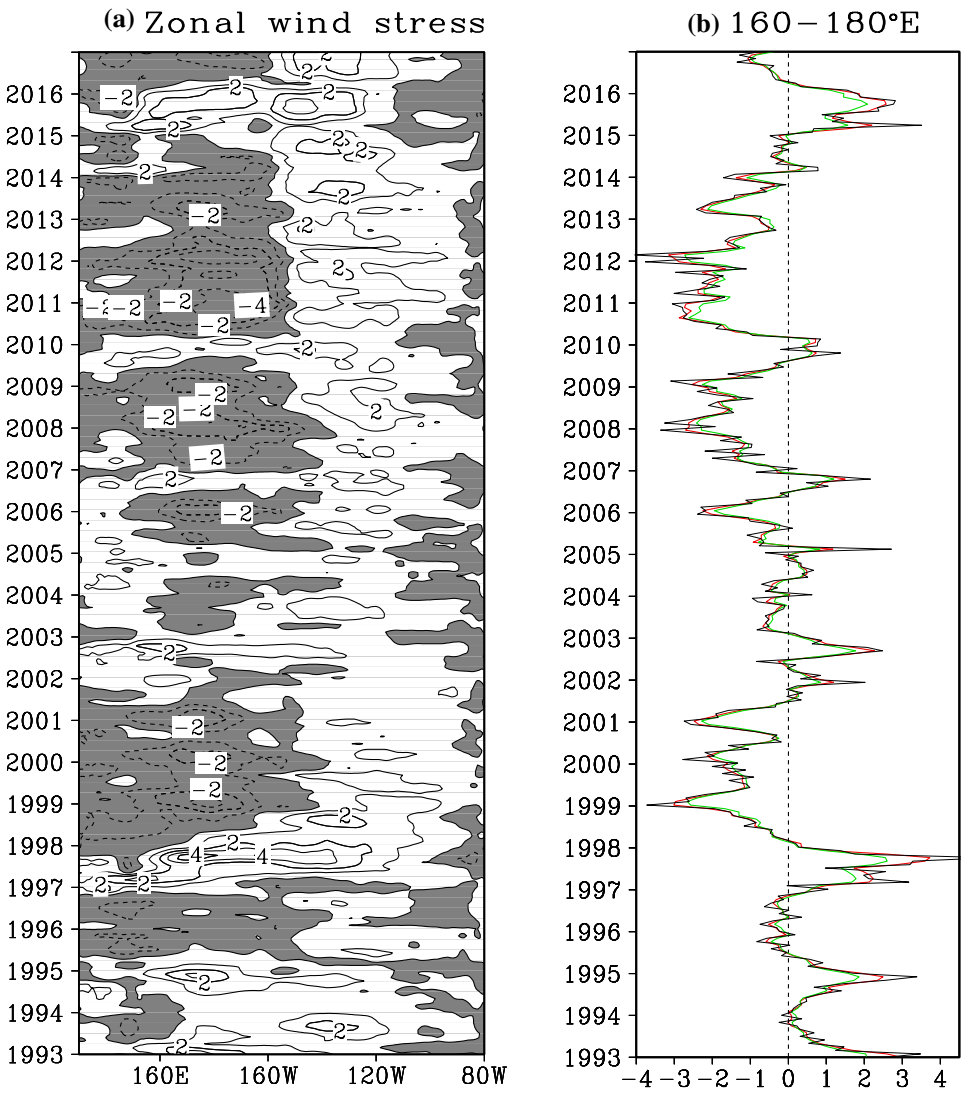

Fig. 5 **a** Monthly zonal wind stress anomalies averaged between 5°S and 5°N along the equator from the daily NCEP data. Contour interval is 2×10^{-2} Pa. Shading indicates negative values. **b** Comparison of monthly anomalies of area-averaged zonal wind stress over the region 160°E–180°E among the unfiltered wind stress (black curve), the low-passed wind stress (red curve), and the wind stress calculated using the low-passed wind velocity (green). Unit is 10^{-2} Pa

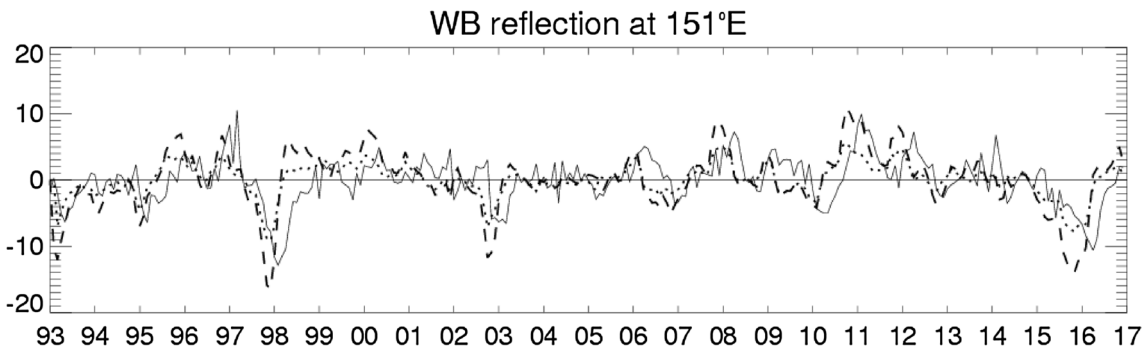

Fig. 6 Coefficients of the decomposed Kelvin waves (solid), linear reflected Kelvin waves calculated from the incoming equatorial Rossby waves of meridional modes 1 and 3 (dotted) and the incoming equatorial Rossby waves of meridional modes 1–3 (dashed) of the first baroclinic mode at the western boundary for the MR

theory suggests that the linear model is deficient in simulating the Rossby wave reflection at the western boundary. This result is consistent with the previous forcing of Yuan et al. (2004).

Large upwelling Rossby waves are evidently reflected into upwelling Kelvin waves at the western boundary during the strongest 1997–1998 and 2015–2016 El Niño events, suggesting that the western boundary reflections play an important role in the termination of the strong El Niño events. However, the onsets of these two largest El Niño events are significantly different. The downwelling Kelvin waves at the western boundary during the onset of the 1997–1998 El Niño are much larger than those during the onset of the 2015–2016 El Niño. During the early stage of the 2015–2016 El Niño, the downwelling Kelvin waves are forced primarily by the westerly winds near the deadline, with very little amplitude of the reflected Kelvin waves coming from the western boundary to propagate to the eastern Pacific (Figs. 4, 5, 6). But in the first few months of 1997, the downwelling Kelvin waves are coming strongly from the western boundary reflection of the equatorial Rossby waves (Fig. 6), which are further strengthened by the westerly winds during the propagation to the east (Figs. 4, 5). The equatorial wave dynamics of the 1997–1998 El Niño with the nonlinearity near the western boundary and in the equatorial Pacific included have been discussed by Yuan et al. (2004). The 2009–2010 El Nino is another strong El Niño event during the period of 1993–2016. But this event is a central-type El Niño (Modoki) and its strength is weaker than the 1997–1998 and 2015–2016 events (Fig. 2). The westerly winds anomalies near the dateline during the 2009–2010 event are significantly weaker than those during the 1997–1998 and 2015–2016 events (Fig. 5), generating weaker upwelling Rossby waves to propagate to the western boundary and weaker upwelling Kelvin waves reflected at the western boundary (Figs. 4, 6). During the decaying stage of the 2009–2010 El Niño, upwelling Kelvin waves are forced by the easterly winds near the deadline (Fig. 5), which are responsible for the termination of the positive SSTA in the central and eastern equatorial Pacific.

The ability of the model to simulate the Kelvin and Rossby waves associated with the ENSO evolution reasonably forms the basis of the analysis of the long-wave dynamics of the intraseasonal rectification in this study.

4 Rectification by the intraseasonal wind forcing

The rectification by the intraseasonal winds is evaluated by comparing the three sensitivity runs with the MR in this section.

4.1 Rectifications of the intraseasonal wind stress on the interannual variability

EXP1 is conducted to force the OGCM with low-pass-filtered wind stress. The SSTA and SLA differences between MR and EXP1 averaged between 5°S and 5°N along the equator are in general less than 0.1 °C and 1 cm, respectively (Fig. 7). The comparison suggests that the rectified SSTA and SLA due to the intraseasonal wind stress forcing are generally small. The rectified SSTA are comparable to the modeled results of Kessler and Kleeman (2000), forced with idealized wind stress. Rong et al. (2011) has also indicated that the effects of the intraseasonal wind stress on low frequency SSTA is small in the Geophysical Fluid Dynamics Laboratory (GFDL) MOM2.2 experiments forced with realistic wind stress.

The MR and EXP1 simulations are decomposed into long equatorial waves. The decomposed coefficients of the equatorial Kelvin and Rossby waves rectified by the intraseasonal wind stress forcing are almost all less than 2 (Fig. 8), corresponding to less than 0.36 cm SLA and 2.6 cm s^{-1} zonal current anomalies for the first baroclinic Kelvin wave and of less than 0.28 cm SLA and 3.2 cm s^{-1} zonal current anomalies for the first baroclinic and first meridional mode Rossby waves. The comparisons suggest that the interannual Kelvin and Rossby waves in the equatorial Pacific can be simulated well by the low-frequency wind stress forcing without the intraseasonal variability. The small amplitudes of the rectified Kelvin and Rossby waves provide a dynamical explanation for the small rectified SSTA and SLA in the eastern equatorial Pacific in comparison to their total interannual anomalies.

During the onset and termination of ENSO events, there are Kelvin waves generated by the intraseasonal wind forcing. Weak downwelling Kelvin waves are generated by the intraseasonal wind forcing at the end of 1994, 1997, 2002, 2006, 2009, and 2015, followed by weak upwelling Kelvin waves at the beginning of 1995, 1998, 2003, 2007, 2010 and 2016. Weak upwelling Kelvin waves are generated by the intraseasonal wind forcing followed by a weak downwelling Kelvin wave during the 1995–1996, 1998–1999, 1999–2000, 2000–2001, 2007–2008, and 2010–2011 cold events. However, their amplitudes (Fig. 8) are much smaller than the interannual anomalies in Fig. 4. Thus, we conclude that the rectification of the intraseasonal wind stress forcing on the interannual oceanic equatorial Kelvin and Rossby waves is generally small.

The coefficients of the decomposed Kelvin waves at the western boundary in EXP1 are nearly the same as those in MR forced with the unfiltered wind stress (Fig. 9). This suggests that the rectification of the intraseasonal wind stress forcing on the interannual oceanic Kelvin waves near the western boundary is much smaller than the Kelvin waves reflected at the Pacific western boundary. Therefore, the western boundary wave reflection plays a more important role in ENSO cycling than the intraseasonal wind stress forcing.

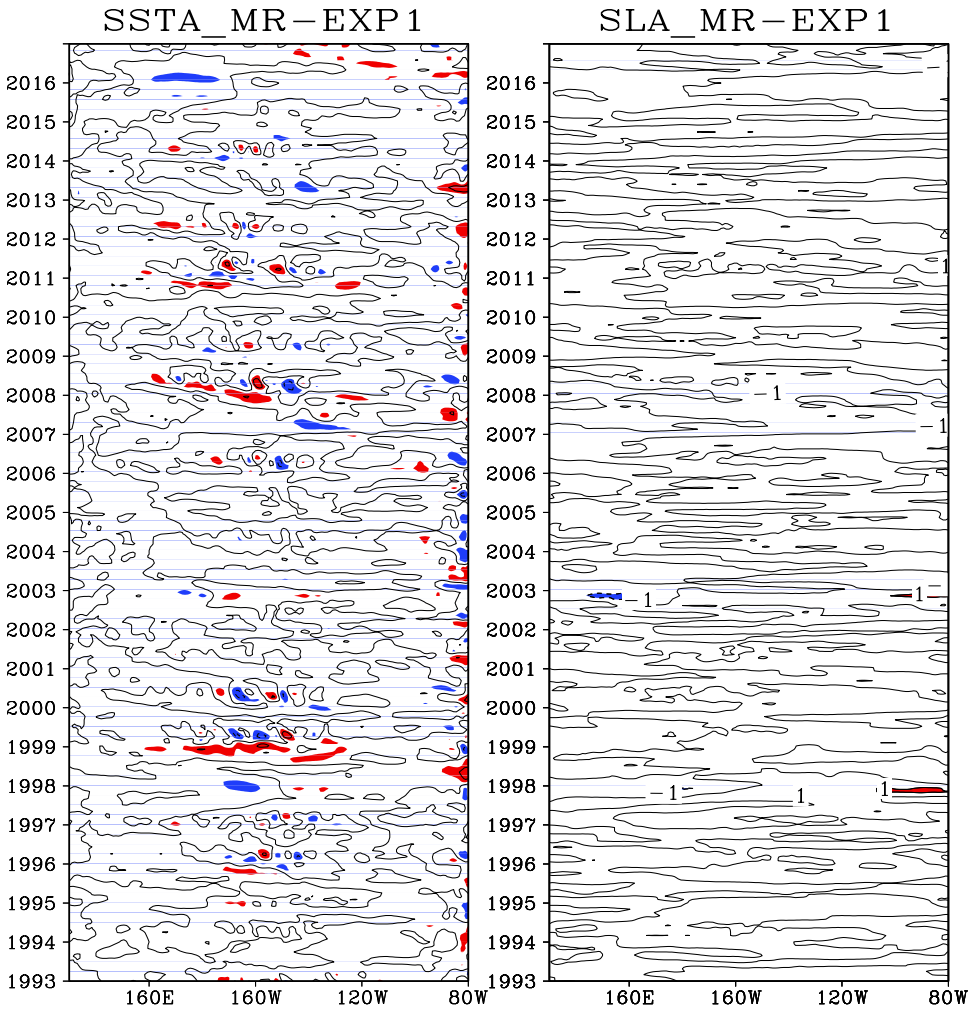

Fig. 7 Monthly SSTA (left) and SLA (right) along the equator averaged between 5°S and 5°N for the difference between MR and EXP1. For the SSTA, red color indicates positive anomalies greater than 0.1 °C, and blue color indicates negative anomalies smaller than −0.1 °C, and the contour interval is 0.2. For the sea level anomalies, red color indicates positive anomalies greater than 1 cm, and blue color indicates negative anomalies smaller than −1 cm, and the contour interval is 1

4.2 Effects of nonlinearity due to the quadratic wind stress bulk formula

One of the nonlinear rectification mechanisms is the nonlinear quadratic bulk formula of the wind stress calculation, which turns out to produce much weaker low-frequency wind stress anomalies than the total interannual variability (Fig. 5b). The rectified wind stress anomalies averaged over the entire equatorial Pacific between 5°N and 5°S are very weak during the 1994–1995 and 1997–1998 El Niños (not shown). The effects of this rectification on oceanic variability are examined in Experiment EXP2, which is forced with the wind stress calculated from low-passed daily wind velocity. Similar to the result of EXP1 (figure omitted), the SSTA in EXP2 compare well with the Hadley Center data in Fig. 2. The differences between MR and EXP2 are slightly larger than those between MR and EXP1, especially in the central and eastern equatorial Pacific during the 1997–1998, 2002–2003 and 2015–2016 El Niño events (Fig. 10). This indicates that the rectified SSTA by the intraseasonal winds are stronger than those forced by the intraseasonal wind stress, which is consistent with the result of Rong et al. (2011). The maximum differences between MR and EXP2 are barely larger than 0.2 °C in the central-eastern equatorial Pacific during the 1997–1998, 2002–2003, and 2015–2016 El Niño events but are all smaller than 0.2 °C in the western equatorial Pacific during other periods, suggesting the travail effects of the rectification by the intraseasonal wind speeds. The rectified SSTA during La Niña events appear much weaker than those during the warm episodes, which is also consistent with the result of Rong et al. (2011). However, Rong et al. (2011) indicated that the intraseasonal rectification may result in a SSTA decrease of 0.2 °C over the eastern Pacific with as large as 0.8 °C SSTA increase in the cold tongue during the mature phase of the strong El Niño events. The rectified SSTA in our experiment are smaller than those of Rong et al. (2011), which may be due to different models. Our result has no significant changes if we should use the wind product and the filtering methods as those of Rong et al. (2011) (figures not shown).

We have repeated the Experiments MR and EXP2, using the algorithm of Rong et al. (2011) to calculate the surface

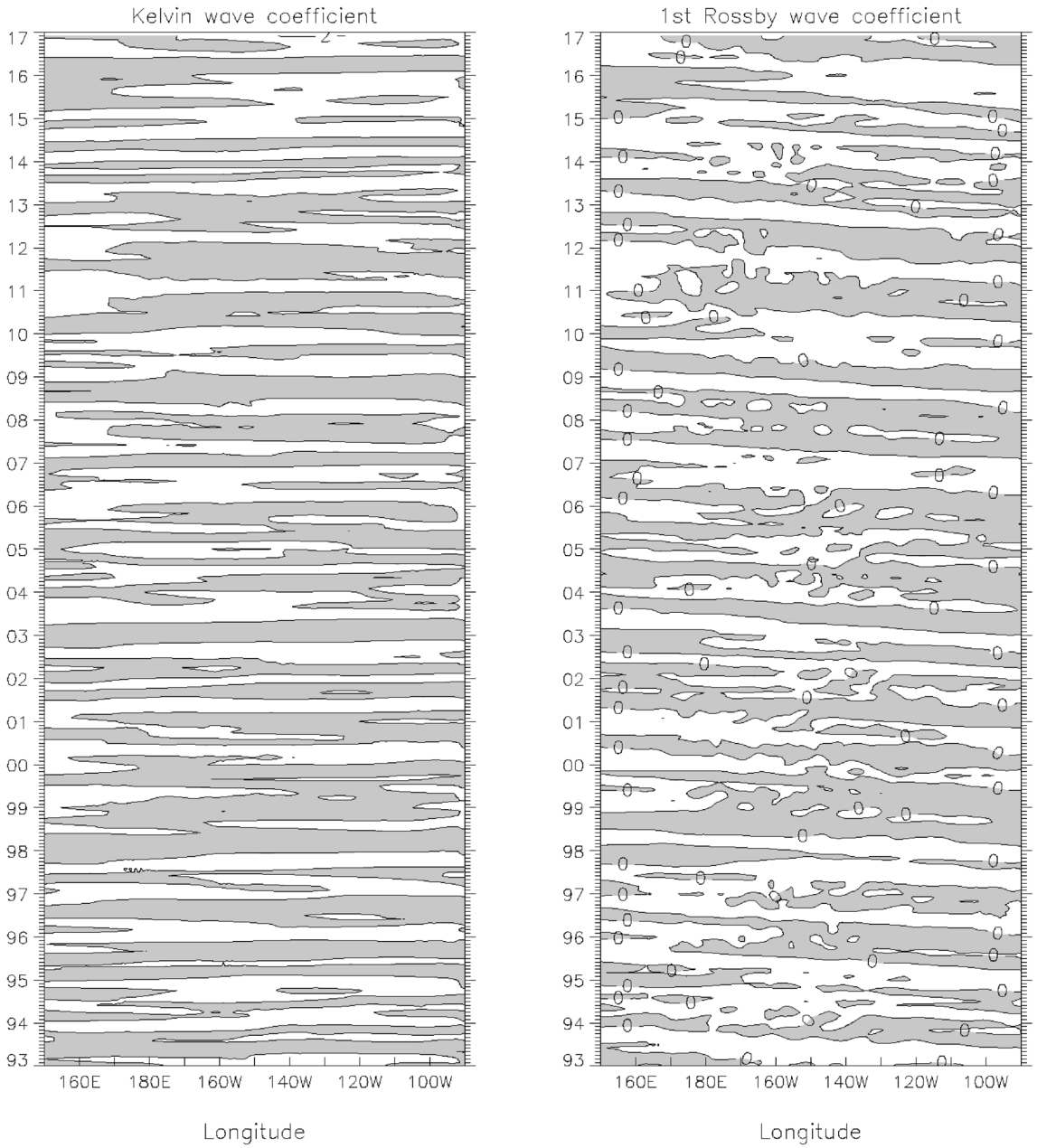

Fig. 8 Decomposed coefficients of equatorial Kelvin and the first meridional mode Rossby waves of the first baroclinic mode for the results of MR-EXP1. Shading indicates the negative values, and the contour interval is 2

latent and sensible heat fluxes. The rectified SSTA are slightly larger but are still significantly weaker than those in Rong et al. (2011) (figures omitted). Either study seems to suggest that the rectified SSTA by the intraseasonal winds are small compared with the full interannual anomalies of ENSO. It is worth mentioning that the heat flux specification in Rong et al. (2011) requires a restoring term to relax the model upper ocean temperature and salinity to the observed. The restoring term has been saved and applied in the control and the sensitivity experiment without the restoring term to produce similar mean state. We think there is still relative drift of the mean state between the control and the sensitivity experiments, which may have resulted in the SSTA to grow faster. In our experiments, the wind stress mean state in EXP2 only differs from that in the MR slightly. Using the daily wind stress climatology from MR and anomalies from EXP2, and the two heat fluxes algorithms, produces small SSTA differences between the two experiments (not shown).

The differences of SLA along the equator averaged between 5°S and 5°N between MR and EXP2 are slightly

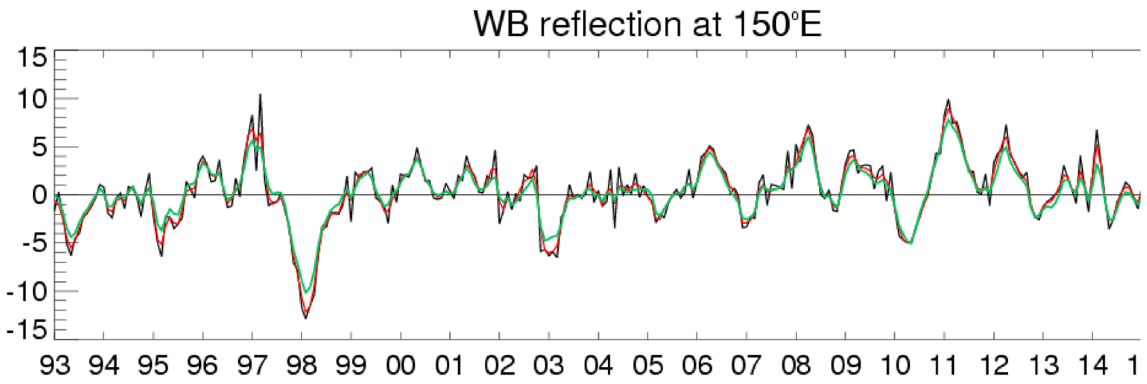

Fig. 9 Coefficients of the decomposed Kelvin waves of the first baroclinic mode at the western boundary for the MR (black curve), the EXP1 (red curve), and the EXP2 (green curve)

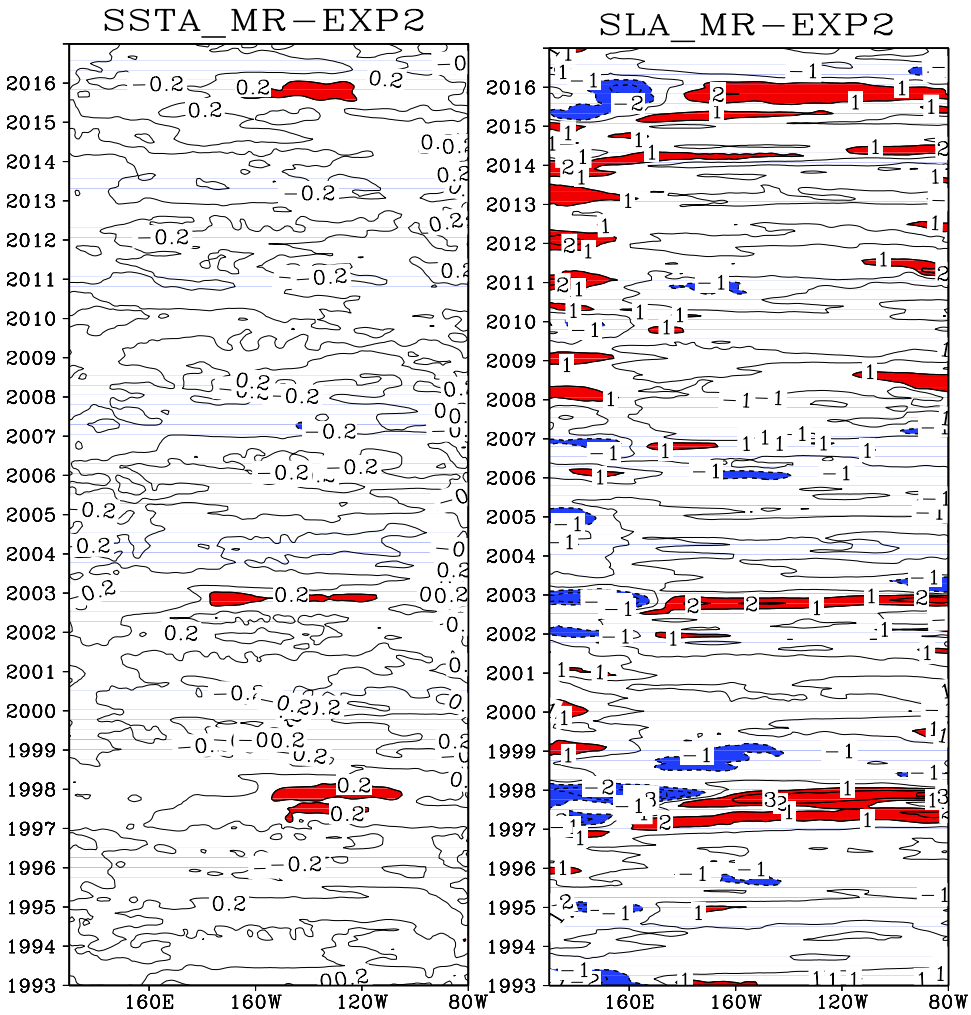

Fig. 10 Monthly SSTA (left) and SLA (right) along the equator averaged between 5°S and 5°N for the difference between MR and EXP2. For the SSTA, red color indicates positive anomalies greater than 0.2 °C, and blue color indicates negative anomalies smaller than −0.2 °C, and the contour interval is 0.2. For the sea level anomalies, red color indicates positive anomalies greater than 1 cm, and blue color indicates negative anomalies smaller than −1 cm, and the contour interval is 1

larger than those between MR and EXP1. Intraseasonal wind forcing represented by the difference between MR and EXP2 has evidently produced positive (negative) SLA in the central-eastern (western) equatorial Pacific during 1997–1998, 2002–2003 and 2015–2016 El Niño events. But the amplitudes are smaller than the total interannual anomalies by nearly an order of magnitude, suggesting the minor effects of the intraseasonal rectification during the El Niño events.

Due to the nonlinear quadratic relationship between the surface wind velocity and the wind tress, decomposed coefficients of the equatorial Kelvin and Rossby waves from the difference between MR and EXP2 (Fig. 11) are slightly larger than those from the difference between MR and EXP1 during the 1997–1998, 2002–2003 and 2015–2016 El Niño events (Fig. 8). But all of the differences are much smaller than the magnitudes of the total interannual equatorial waves in Fig. 4. Nor are the western boundary wave reflection altered significantly by the intraseasonal winds as indicated by the comparison of the decomposed Kelvin waves at the western boundary in MR and EXP2 (Fig. 9).

4.3 Rectification by intraseasonal heat flux associated with the intraseasonal winds

Besides the dynamical forcing by the intraseasonal wind stress, the intraseasonal heat fluxes associated with passages of the intraseasonal events force the model thermodynamics. To estimate the effects of intraseasonal heat fluxes on the

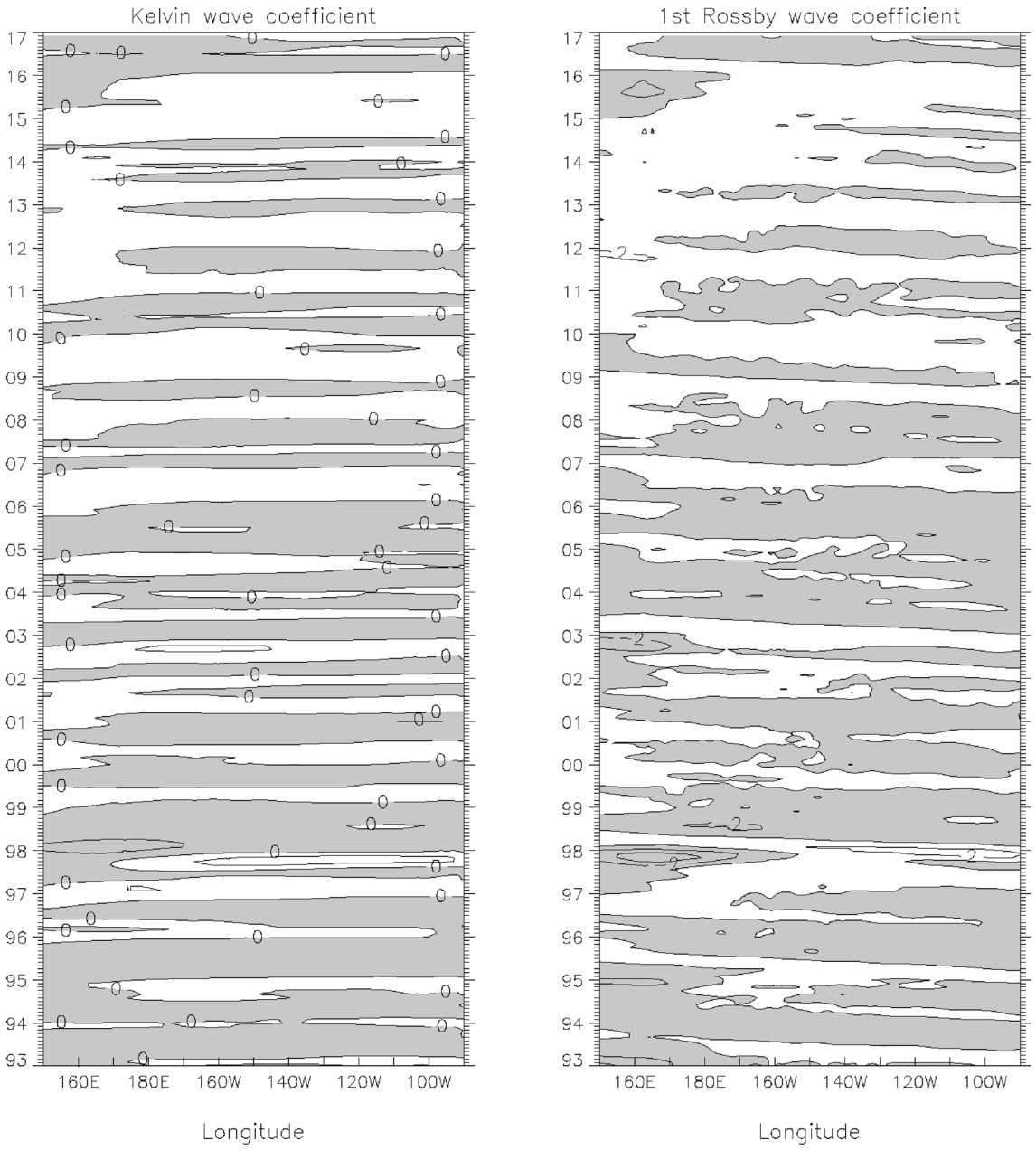

Fig. 11 Decomposed coefficients of equatorial Kelvin and the first meridional mode Rossby waves of the first baroclinic mode for the results of MR-EXP2. Shading indicates the negative values, and the contour interval is 2

interannual SST and equatorial wave dynamics of ENSO, Experiment EXP3 is conducted to use low-pass-filtered daily wind to calculate the surface wind stress, as well as the latent and sensible heat fluxes. The difference between EXP2 and EXP3 measures the impact of intraseasonal heat flux associated with the intraseasonal winds. Sizable differences of the SSTA between EXP2 and EXP3 are identified, the absolute values of which are greater than 0.2 °C only in the western equatorial Pacific and are generally smaller than 0.2 °C in the eastern equatorial Pacific (Fig. 12). This comparison suggests that SSTA in the western equatorial Pacific are more sensitive to the rectification of the intraseasonal heat flux forcing than to the intraseasonal wind stress forcing. During the 1994–1995, 1997–1998, 2002–2003, 2006–2007, 2009–2010, and 2015–2016 El Niño events, the atmospheric convection center moves eastward, bringing the intraseasonal wind variability with it, which rectifies negative SSTA in the western-central equatorial Pacific Ocean. The opposite occurs during the 1995–1996, 1998–1999, 1999–2000, 2000–2001, 2007–2008, and 2010–2011 La Niña events so that positive SSTA are rectified in the western equatorial Pacific Ocean. Thus, the intraseasonal heat fluxes induce SSTA anomalies in the western-central equatorial Pacific that enhance the anomalous zonal SST gradient over the equatorial Pacific Ocean during ENSO events.

The numerical experiments of Kessler and Kleeman (2000), forced with idealized MJO winds, show that the overall signature of the rectified anomalies was low-frequency SST cooling in the western Pacific under strong winds of either sign (bottom left of their Fig. 3). Compared with the difference between MR and EXP1 (EXP2), the SSTA in the western-central equatorial Pacific due to heat flux rectification are larger than these due to the wind stress rectification, owing to the existence of the barrier layer under the surface mixed layer (Figs. 7, 10, 12). In the eastern Pacific, the intraseasonal wind variability is very weak. The interannual SSTAs in the eastern equatorial Pacific are dominated by the Kelvin waves because of the absence of the barrier in the east and the sensitivity of the SST to the thermocline variability. Thus, the SSTA in the central-western equatorial Pacific are dominated by the intraseasonal heat flux rectification, whereas those in the eastern equatorial

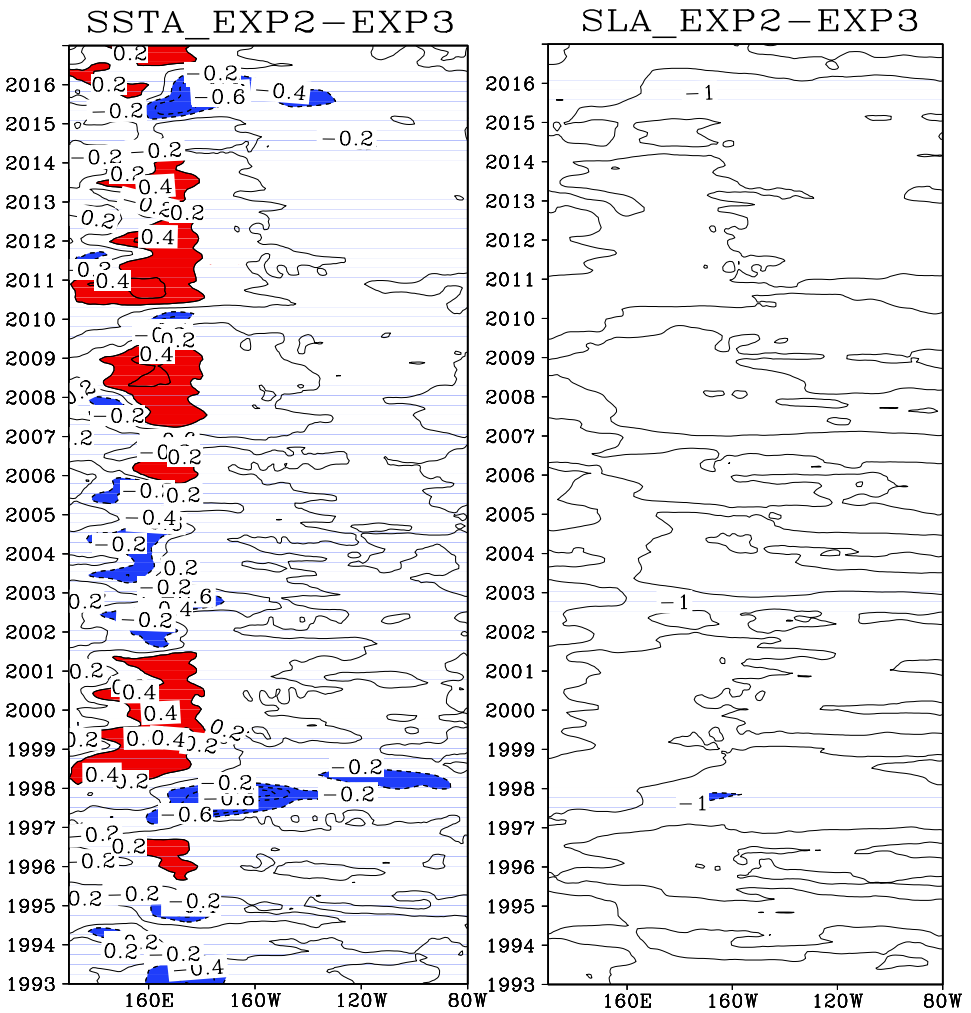

Fig. 12 Monthly SSTA (left) and SLA (right) along the equator averaged between 5°S and 5°N for the difference between EXP2 and EXP3. For the SSTA, red color indicates positive anomalies greater than 0.2 °C, and blue color indicates negative anomalies smaller than −0.2 °C, and the contour interval is 0.2. For the sea level anomalies, red color indicates positive anomalies greater than 1 cm, and blue color indicates negative anomalies smaller than −1 cm, and the contour interval is 1

Pacific are dominated by the Kelvin waves rectified by the intraseasonal wind stress in the central-western Pacific.

The SLA between EXP2 and EXP3 do not show nearly as much difference as the SSTA do. This comparison suggests that the rectification by the intraseasonal heat fluxes has little influence on the oceanic dynamical process. The equatorial Kelvin and Rossby waves from the difference between EXP2 and EXP3 are also much smaller than the total interannual waves (not shown), suggesting that the sensitivity of the heat flux rectification is confined in the western Pacific, which do not propagate to the eastern equatorial Pacific to generate significant SSTA in the cold tongue.

Notice that, since the model is forced with observed wind stress, the coupled effects due to the rectification have already into the hindcast experiments, so that the sensitivity tests have all of the coupled effects included.

5 Role and dynamics of the intraseasonal rectification

The daily output from Experiments MR and EXP1 is used to calculate the nonlinear advection terms in the zonal momentum equation for the period of January 1997 through December 1998 (Fig. 13). All terms are moved to the right side of the equation and integrated above the thermocline depth (20 °C isotherm depth). The current anomalies are in reference to the monthly climatology for the period of 1993–2016. Daily advection anomalies are calculated from the current anomalies, which represent the interannual variations of the intraseasonal advection. These advection anomalies are found to contain primarily intraseasonal variabilities at 25–60 day periods according to the power spectrum (not shown), with very small semi-annual and annual

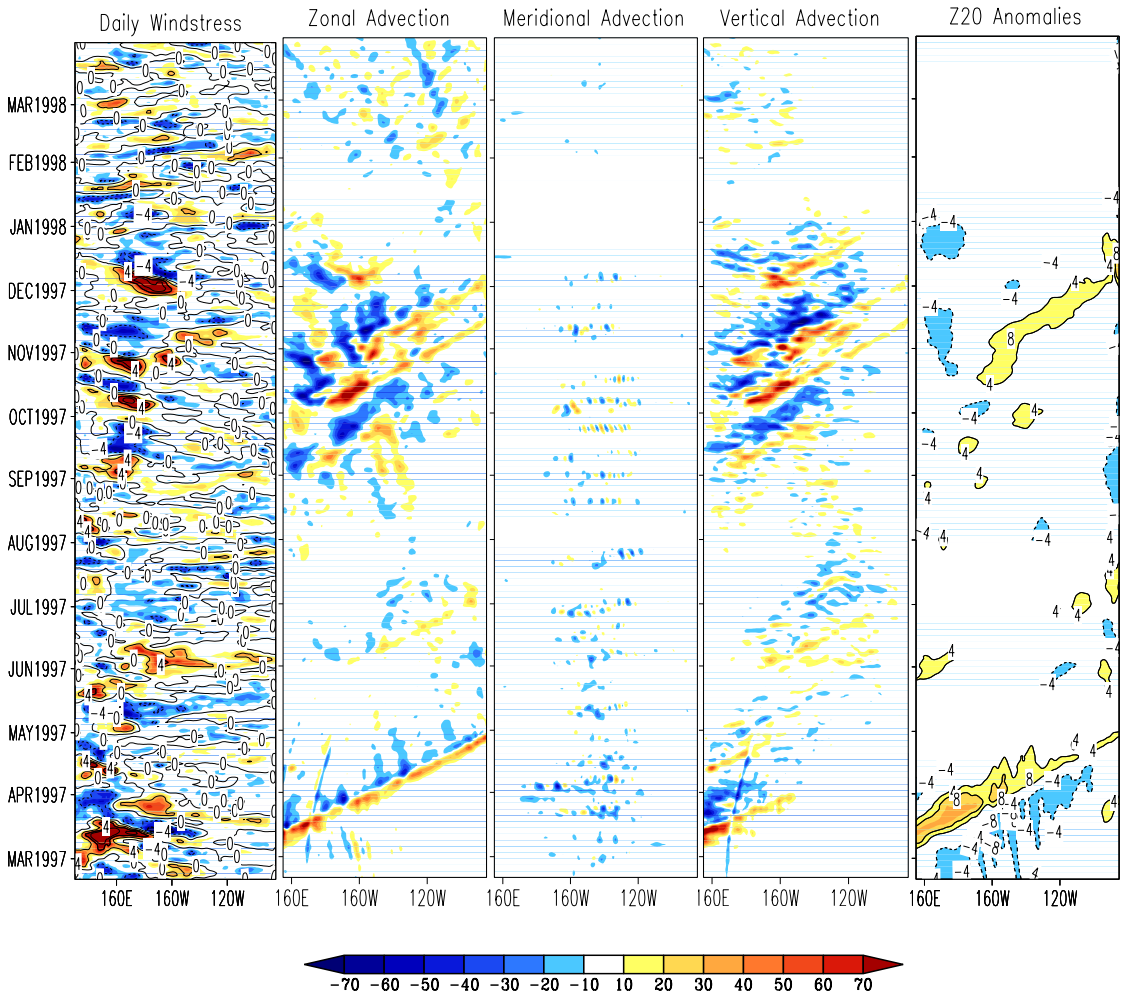

Fig. 13 Daily zonal windstress anomalies (unit: 10^{-2} Pa), zonal, meridional, and vertical advection anomalies of zonal current above the thermocline (unit: 10^{-6} ms^{-2}), and Z20 anomalies (unit: m) for the difference between MR and EXP1. The meridional advection anomalies are averaged between 0° and 5°N, and others are averaged between 5°S and 5°N

variability, suggesting the successful removal of the seasonal climatology.

The strong MJO events in early 1997 and in October–December 1997 have generated weak downwelling Kelvin waves to the eastern equatorial Pacific Ocean, as indicated by the depth anomalies of the 20 °C isotherm (Fig. 13). The nonlinear advection terms suggest that the rectification is dominated by the zonal and vertical advection, with the meridional advection much smaller than the zonal and vertical advection. The low-passed zonal and vertical advection terms are confirmed to be much larger than the meridional advection (figure omitted). These advection anomalies suggest clearly that the intraseasonal rectification is not due to the surface Ekman transports. The downwelling Kelvin waves neither support the thermocline rectification hypothesis. An examination of the background equatorial currents (not shown) reveals that the nonlinear advection is due to the low-frequency zonal and vertical currents, which have become positive (eastward and upward) since March 1997. The positive background currents give rise to the positive advection of the zonal momentum after the intraseasonal forcing has passed through, hence the rectified downwelling equatorial Kelvin waves to the east. During La Niña events, say in 1998, the low-frequency equatorial zonal currents are to the west, but the MJO is weak in the western Pacific, so that the rectified Kelvin waves are weak.

The rectified Kelvin waves are much weaker than the reflected Kelvin waves at the western boundary (compare Figs. 4, 8, 11). In addition, the rectified Kelvin waves east of the dateline are found much weaker than those forced by the low-frequency winds without the intraseasonal components (Fig. 14). The small amplitudes of the rectified equatorial Kelvin waves suggest that the intraseasonal rectification unlikely play an important role in the onset and evolution dynamics of the El Niño event.

6 Summary and discussions

The rectification of intraseasonal wind forcing on the SSTA and SLA associated with ENSO during 1993–2016 are investigated using the LICOM OGCM forced with the daily winds of the NCEP-NCAR reanalysis with and without the intraseasonal variations, respectively. The effects of the rectification by the intraseasonal wind velocity through the nonlinearity of the stress bulk formula, and by the intraseasonal heat flux induced by the intraseasonal winds, are also investigated.

In the Experiment MR forced with the daily wind stress and heat flux of the NCEP–NCAR reanalysis, the simulated SSTA and SLA in the equatorial Pacific Ocean are in good agreement with the observed SSTA of the Hadley Center and the SLA of the AVISO satellite altimeter during 1993–2016. The model simulated equatorial Kelvin and Rossby waves explain the ENSO evolution and cycling reasonably, suggesting that the model can be used as a proxy to investigate the long-wave dynamics of the intraseasonal wind forcing on ENSO.

The simulated SLA during the 1997–1998 and the 2015–2016 strong El Niño are weaker than the altimeter data, which may be due to errors of the wind stress or/and model dynamics. This deficiency seems to be a common problem of modern ENSO simulations [c.f. the NASA simulation in Yuan et al. (2004)]. The ocean state estimate by the Estimating the Circulation and Climate of the Ocean Phase II (ECCO2) system, which is obtained by least squares fitting of the Massachusetts Institute of Technology general circulation model (MITgcm) to the available satellite and in-situ observations, also shows a weaker SLA during 2015–2016 (left panel of Fig. 15). Furthermore, using the ERA-interim reanalysis winds of the European Centre for Medium-Range Weather Forecasts (ECMWF, Dee et al. 2011) to force the LICOM model used in the present paper gives a similar result (right panel of Fig. 15).

The rectification of the intraseasonal wind stress forcing on the interannual SSTA and SLA is found much weaker than the total interannual SSTA and SLA. Using the ERA-interim reanalysis data to force the model gives a similar result (not shown). The dynamics of the weak rectification is due to the weakly rectified interannual Kelvin and Rossby waves in the equatorial Pacific Ocean. The rectified interannual Kelvin waves are found to be much smaller than that reflected at the Pacific western boundary or forced by the low-frequency winds, suggesting that the latter two play a more important role in the ENSO cycling and termination.

The nonlinear advection of the ocean in 1997 is analyzed, showing dominance of the zonal and vertical advection over the meridional advection in the zonal momentum equation (Fig. 13). The negligible meridional advection suggests that the surface Ekman transport is not the primary dynamics controlling the intraseasonal rectification. The variations of the 20 °C depth are very small, showing that the intraseasonal rectification is not controlled by the thermocline rectification, either. A downwelling Kelvin wave is rectified after a MJO cycle, because the background currents in the western Pacific is eastward and downward during 1997.

The intraseasonal heat flux associated with the intraseasonal winds is found to produce slightly larger SSTA in the western-central equatorial Pacific Ocean than in the east. Abnormal coolings (warmings) are generated in the western-central equatorial Pacific during strong El Niño (La Niña) events, enhancing (reducing) the zonal SST gradient over the equatorial Pacific Ocean. However, the magnitudes of the rectified SSTA are much smaller than the total SSTA, suggesting minor roles of the intraseasonal rectification. Most importantly, the rectification of the intraseasonal heat

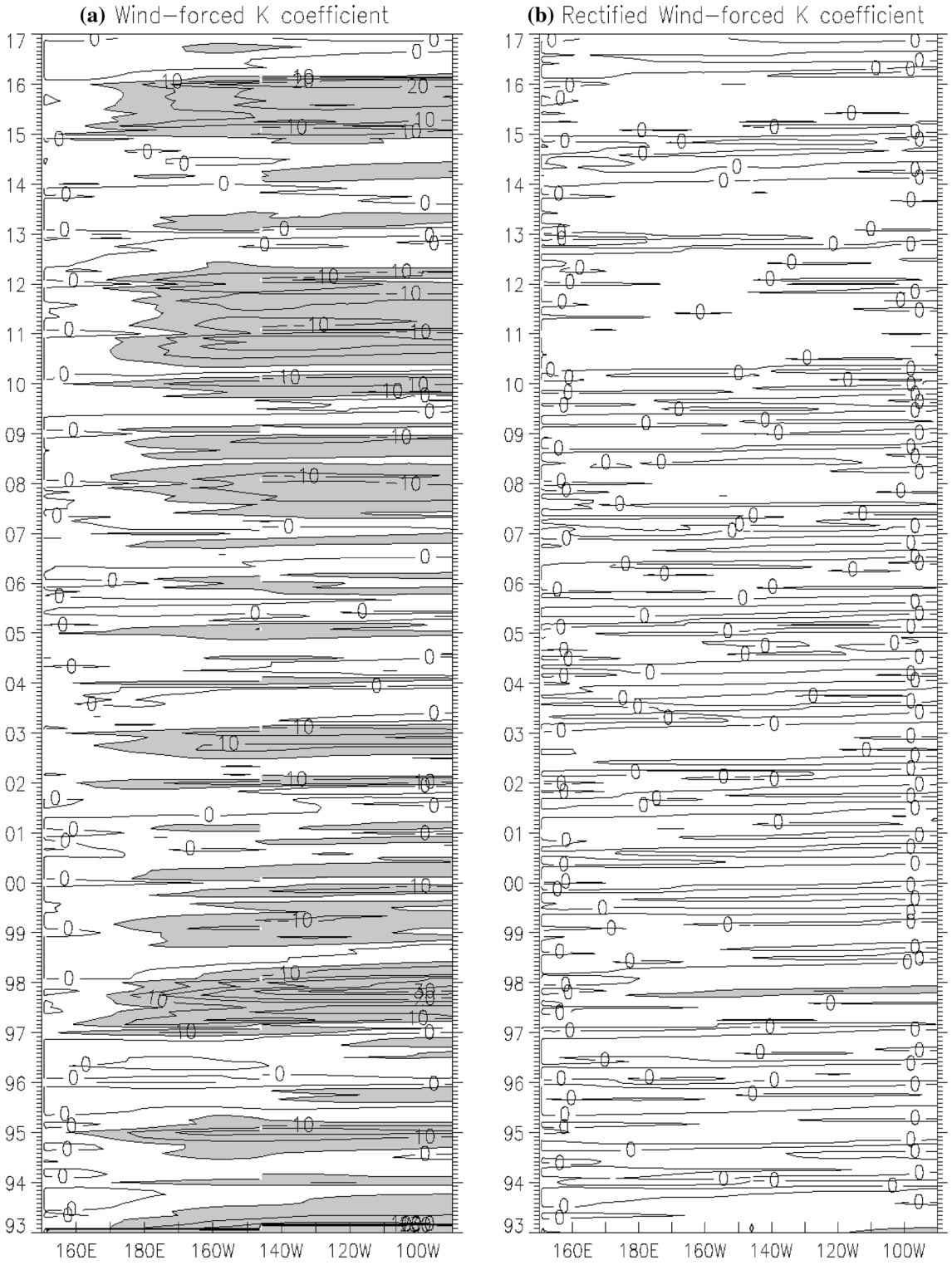

Fig. 14 **a** Wind-forced Kelvin wave coefficients with western boundary wave condition at 151°E set to zero. **b** Same as left but forced by the intraseasonal wind stress. Shading indicates the values greater (smaller) than 5 (−5)

flux on the interannual SLA is negligibly small, generating negligibly small equatorial Kelvin waves to propagate to the eastern equatorial Pacific.

The numerical experiments conducted in this study suggest that the intraseasonal winds generate very weak interannual equatorial Kelvin waves to propagate to the eastern

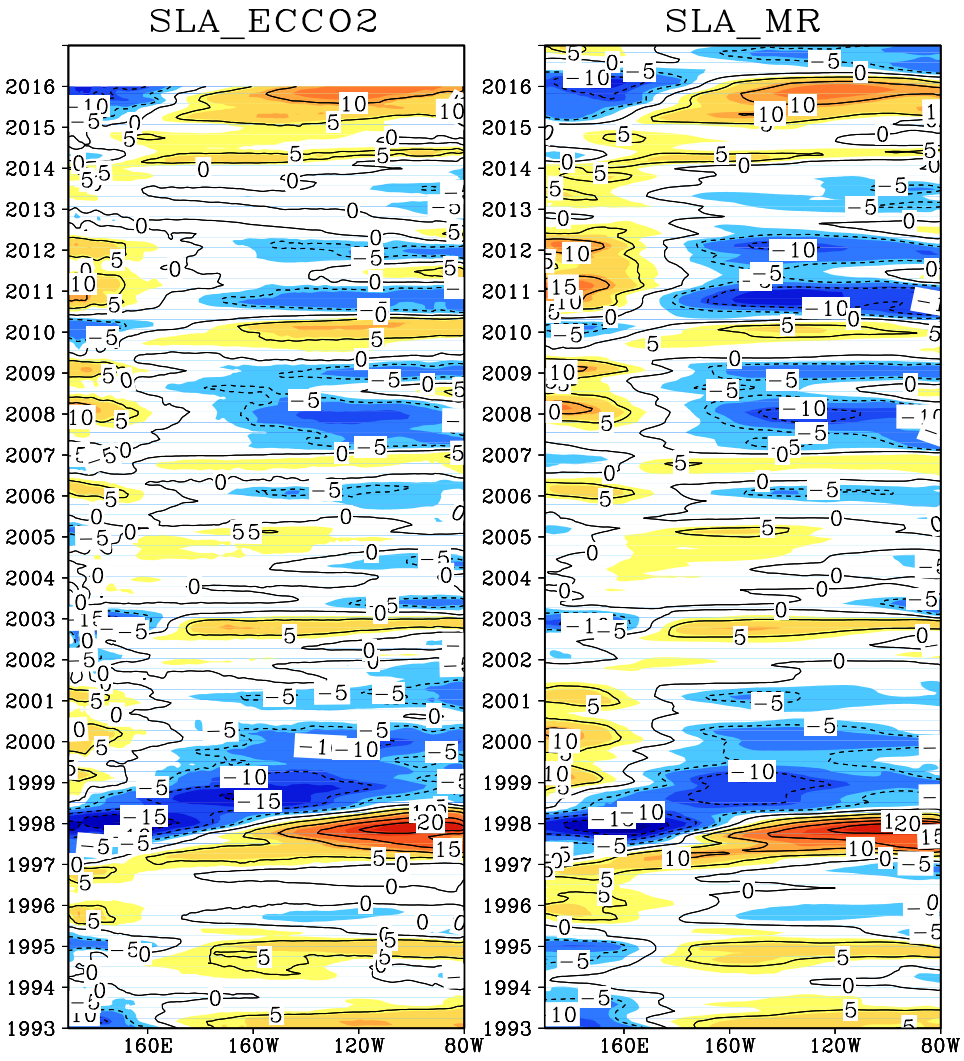

Fig. 15 Monthly SLA between 5°S and 5°N of the ECCO2 (left panel) and the MR of the LICOM model using the wind forcing of the ERA-interim data (right panel). Red (blue) color indicates SLA greater (less) than 3 (−3) cm, and the contour interval is 5 cm

equatorial Pacific. This fact suggests that the anomalous warming or cooling of the cold tongue during ENSO is unlikely forced by the dynamical rectification of the ocean driven by the intraseasonal winds. The weak SSTA rectified by the intraseasonal winds in comparison with the total interannual SSTA also suggest weak response of the atmospheric Walker Cell circulation. The rectified equatorial Kelvin waves are much weaker than those forced by the low-frequency winds and reflected at the Pacific western boundary, suggesting the insignificance of the intraseasonal rectification in the ENSO cycling.

It is worth noting that the nonlinear dynamics of the western boundary currents (Yuan and Wang 2011; Wang and Yuan 2012, 2014) are not analyzed in this study in the LICOM simulation. Strong nonlinearity of the western boundary currents and regime shifts of the ocean currents at the Pacific entrance of the Indonesian Seas due to the existence of multiple equilibria could induce significant Kelvin waves in the far western equatorial Pacific Ocean (Yuan et al. 2018). Due to the coarse resolution of the LICOM model used in this study, these aspects of the oceanic nonlinearity are not investigated. There is also a potential role for the stochastic forcing to induce variability at ENSO time scales through the so-called linear stability mechanism of the coupled system (e.g. Moore and Kleeman 1999). The rectification of intraseasonal wind forcing on ENSO should be further studied using a coupled model.

Acknowledgements This work was supported jointly by NSFC (41421005, 41375094, 41406028, 41720104008, 41776011), QMSNL (2016ASKJ12), CAS (XDA11010102, XDA11010205), and the Shandong Provincial projects (U1406401). We thank the Aviso project, Hadley Center, and NCEP for sharing their data.

References

Bergman JW, Hendon HH, Weickmann KM (2001) Intraseasonal air–sea interactions at the onset of El Niño. J Clim 14:1702–1719

Boulanger JP, Menkes C (1999) Long equatorial wave reflection in the Pacific Ocean from TOPEX/POSEIDON data during the 1992–1998 period. Clim Dyn 15:205–225

Boulanger JP, Cravatte S, Menkes C (2003) Reflected and locally wind-forced interannual equatorial Kelvin waves in the western Pacific Ocean. J Geophys Res 108(C10):3311. https://doi.org/10.1029/2002JC001760

Chen D, Lian T, Fu C, Cane MA, Tang Y, Murtugudde R et al (2015) Strong influence of westerly wind bursts on El niño diversity. Nat Geosci 8:339–345

Dee DP et al (2011) The ERA-Interim reanalysis: configuration and performance of the data assimilation system. Q J R Meteorol Soc 137:553–597. https://doi.org/10.1002/qj.828

Fedorov AV, Hu S, Lengaigne M, Guilyardi E (2014) The impact of westerly wind bursts and ocean initial state on the development, and diversity of El Niño events. Clim Dyn 44:1381

Hendon HH, Zhang C, Glick JD (1999) Interannual variation of the Madden–Julian oscillation during austral summer. J Clim 12:2538–2550

Hendon HH, Wheeler MC, Zhang C (2007) Seasonal dependence of the MJO–ENSO relationship. J Clim 20:531–543

Hu S, Fedorov AV (2016) Exceptionally strong easterly wind burst stalling El Niño of 2014. (EARTH, ATMOSPHERIC AND PLANETARY SCIENCES) (Report). In: Proceedings of the National Academy of Sciences of the United States, vol 113(8), 2005

Jin FF (1997a) An equatorial ocean recharge paradigm for ENSO. Part I: conceptual model. J Atmos Sci 54:811–829

Jin FF (1997b) An equatorial ocean recharge paradigm for ENSO. Part II: a stripped-down coupled model. J Atmos Sci 54:830–847

Kalnay et al (1996) The NCEP/NCAR 40-year reanalysis project. Bull Am Meteorol Soc 77:437–470

Kessler WS, Kleeman R (2000) Rectification of the Madden–Julian oscillation into the ENSO cycle. J Clim 13:3560–3575

Kessler WS, McPhaden MJ, Weickmann KM (1995) Forcing of intraseasonal Kelvin waves in the equatorial Pacific. J Geophys Res 100:10613–10631

Large WG, Yeager SG (2004) Diurnal to decadal global forcing for ocean and sea-ice models—the data sets and flux climatologies NCAR Technical Note NCAR/TN-460 + STR

Large WG, Yeager SG (2009) The global climatology of an interannually varying air–sea flux data set. Clim Dyn 33:341–364

Lengaigne M, Guilyardi E, Boulanger JP, Menkes C, Delecluse P, Inness P, Cole J, Slingo J (2004a) Triggering of El Nino by westerly wind events in a coupled general circulation model. Clim Dyn 23(6):601–620

Lengaigne M, Boulanger JP, Menkes C, Delecluse P, Slingo J (2004b) Westerly wind events in the tropical Pacific and their influence on the coupled ocean–atmosphere system: a review. In: Wang C, Xie SP, Carton JA (eds) Earth's climate: the ocean–atmosphere interaction. Geophys Monogr Ser, vol 147. AGU, Washington, D. C, pp 49–69

Levitus S, Boyer TP (1994) World Ocean Atlas 1994 Volume 4: Temperature. NOAA Atlas NESDIS 4. U.S. Department of Commerce, Washington, DC, p 117

Levitus S, Burgett R Boyer TP (1994). World Ocean Atlas 1994 Volume 3: Salinity. NOAA Atlas NESDIS 3. U.S. Department of Commerce, Washington, DC, p 99

Liu H, Yu Y, Li W, Zhang X (2004) LASG/IAP climate system ocean model (LICOM1.0), User manual (in Chinese). Science Publication, Washington, DC

Liu H, Li W, Zhang X (2005) Climatology and variability of the Indonesian throughflow in an eddy-permitting oceanic GCM. Adv Atmos Sci 22:496–508

Lukas R, Lindstrom E (1991) The mixed layer of the western equatorial Pacific Ocean. J Geophys Res 96:3343–3357. https://doi.org/10.1029/90JC01951

Lukas R, Hayes SP, Wyrtki K (1984) Equatorial sea level response during the 1982–1983 El Niño. J Geophys Res 89:10425–10430

Luther DS, Harrison DE, Knox RA (1983) Zonal winds in the central equatorial pacific and El niño. Science 222:327–330

Madden R, Julian P (1971) Detection of a 40–50 day oscillation in the zonal wind in the tropical Pacific. J Atmos Sci 28:702–708

Madden R, Julian P (1972) Description of global-scale circulation cells in the tropics with a 40–50 day period. J Atmos Sci 29:1109–1123

McPhaden MJ (1999) Genesis and evolution of the 1997– 98 El Niño. Science 283:950–954

Menkes CE, Lengaigne M, Vialard J, Puy M, Marchesiello P, Cravatte S, Cambon G (2014) About the role of westerly wind events in the possible development of an El Niño in 2014. Geophys Res Lett 41(18):6476–6483

Moore AM, Kleeman R (1999) Stochastic forcing of ENSO by the intraseasonal oscillation. J Clim 12:1199–1220

Packnowski RC, Philander SGH (1981) Parameterization of vertical mixing in numerical models of the tropical ocean. J Phys Oceanogr 11:1442–1451

Picaut J, Masia F, Penhoat Y (1997) An advective-reflective conceptual model for the oscillatory nature of the ENSO. Science 277:663–666

Rayner NA, Parker DE, Horton EB, Folland CK, Alexander LV, Rowell DP, Kent EC, Kaplan A (2003) Global analyses of sea surface temperature, sea ice, and night marine air temperature since the late nineteenth century. J Geophys Res 108:4407. https://doi.org/10.1029/2002JD002670

Rong X, Zhang R, Li T, Su J (2011) Upscale feedback of high-frequency winds to ENSO. Q J R Meteorol Soc 137:894–907

Roundy PE, Kiladis GN (2006) Observed relationships between intraseasonal oceanic Kelvin waves and atmospheric forcing. J Clim 19:5253–5272

Schopf PS, Suarez MJ (1988) Vacillations in a coupled oceanatmosphere model. J Atmos Sci 45:549–566

Shinoda T, Roundy PE, Kiladis GN (2008) Variability of intraseasonal kelvin waves in the equatorial Pacific Ocean. J Phys Oceanogr 38:921–944. https://doi.org/10.1175/2007JPO3815.1

Slingo J, Rowell DF, Sperber KR, Nortley F (1999) On the predictability of interannual behavior of the Madden–Julian Oscillation and its relationship to El Niño. Q J R Meteorol Soc 125:583–609

Suarez MJ, Schopf PS (1988) A delayed action oscillator for ENSO. J Atmos Sci 45:3283–3287

Wang Z, Yuan D (2012) Nonlinear dynamics of two western boundary currents colliding at a gap. J Phys Oceanogr 42:2030–2040. https://doi.org/10.1175/JPO-D-12-05.1

Wang Z, Yuan D (2014) Multiple equilibria and hysteresis of two unequal-transport western boundary currents colliding at a gap. J Phys Oceanogr 44(7):1873–1885

Weisberg RH, Wang C (1997) Awestern Pacific oscillator paradigm for the El Nino–Southern Oscillation. Geophys Res Lett 24(7):779–782

Yuan D, Liu H (2009) Long wave dynamics of sea level variations during Indian Ocean dipole events. J Phys Oceanogr 39:1115–1132

Yuan D, Wang Z (2011) Hysteresis and dynamics of a western boundary current flowing by a gap forced by impingement of

mesoscale eddies. J Phys Oceanogr 41:878–888. https://doi.org/10.1175/2010JPO4489.1

Yuan D, Rienecker MM, Schopf PS (2004) Long wave dynamics of the interannual variability in a numerical hindcast of the equatorial Pacific Ocean circulation during the 1990s. J Geophys Res 109:C05019. https://doi.org/10.1029/2003JC001936

Yuan DL, Xiang Li, Wang Z, Yao Li, Wang J, Yang Y, Xiaoyue H, Shuwen T, Hui Z et al (2018) Observed transport variations in the Maluku Channel of the Indonesian Seas associated with western boundary current changes. J Phys Oceanogr. https://doi.org/10.1175/JPO-D-17-0120.1

Zebiak SE (1989) On the 30–60 day oscillation and the prediction of El Niño. J Clim 2:1381–1387

Zhang CD, Gottschalck J (2002) SST anomalies of ENSO and the Madden–Julian oscillation in the equatorial Pacific. J Clim 15:2429–2445

Affiliations

Xia Zhao[1,2] · Dongliang Yuan[1,2,5] · Guang Yang[3,4] · Jing Wang[1,2] · Hailong Liu[6] · Renhe Zhang[7] · Weiqing Han[8]

1 CAS Key Laboratory of Ocean Circulation and Waves, Institute of Oceanology, Chinese Academy of Sciences and Pilot National Laboratory for Marine Science and Technology (Qingdao), Qingdao, China

2 Center for Ocean Mega-Science, Chinese Academy of Sciences, Qingdao, China

3 Center for Ocean and Climate Research, First Institute of Oceanography, State Oceanic Administration, Qingdao, China

4 Laboratory for Regional Oceanography and Numerical Modeling, Qingdao National Laboratory for Marine Science and Technology, Qingdao, China

5 University of Chinese Academy of Sciences, Beijing 100049, China

6 National Key Laboratory of Numerical Modeling for Atmospheric Sciences and Geophysical Fluid Dynamics, Institute of Atmospheric Physics, Chinese Academy of Sciences, Beijing, China

7 Institute of Atmospheric Sciences, Fudan University, Shanghai, China

8 Department of Atmospheric and Oceanic Sciences, University of Colorado, Boulder, USA